AIAA AVIATION Forum
August 2-6, 2021, VIRTUAL EVENT
AIAA AVIATION 2021 FORUM

10.2514/6.2021-2238

Solution of Pierce's equation for Tam & Auriault's mixing noise model

Étienne Spieser* and Christophe Bailly†
Univ Lyon, École Centrale de Lyon, CNRS, Univ Claude Bernard Lyon 1, INSA Lyon, LMFA, UMR5509, 69130, Écully, France

César Legendre‡
Free Field Technologies (part of Hexagon's Manufacturing Intelligence division), Axis Park Louvain-la-Neuve, 9 rue Émile Francqui, B-1435 Mont-Saint-Guibert, Belgium

The adjoint method introduced by Tam & Auriault [1] enables to properly taking into account the acoustic propagation effects when jet noise is modelled from the statistics of a turbulent flow. This technique is recast in a systematic way valid for arbitrary propagation media, linear operators and sound sources. An acoustic analogy based on Pierce's wave equation for the acoustic potential [2] is proposed in this study. Tam & Auriault's mixing noise model [3] is reformulated for this operator. This approach presents three main advantages; no instability wave can occur since the acoustic energy conservation is enforced, then for being self-adjoint the adjoint solution to the propagation problem may straightforwardly be computed by flow reversal, finally Pierce's wave equation is a simple and computationally efficient equation that several existing solvers are able to solve. Work performed with *Actran TM* software is presented illustrating the ability of a commercial tool to solve this equation and to compute adjoint Green's function required in statistical jet noise modelling. The nighty-degree acoustic spectrum of a $M_j = 0.9$ round jet is computed with Green's functions properly tailored to the jet mean flow.

I. Nomenclature

a_0	=	speed of sound
$a_{C,0}$	=	customised speed of sound provided as entry of *Actran TM*
a_∞	=	ambient speed of sound
B	=	fluctuating stagnation enthalpy
b	=	normalised fluctuating stagnation enthalpy
c	=	parameter to model the sound source intercorrelation introduced by Tam & Auriault [3]
D_f	=	fan flow exit diameter
$\mathrm{D}/\mathrm{D}t$	=	$\partial/\partial t + \boldsymbol{u}_0 \cdot \nabla$ material derivative along the mean flow
$\mathrm{D}/\mathrm{D}t_i, \boldsymbol{x}_j$	=	$\partial/\partial t_i + \boldsymbol{u}_0 \cdot \partial/\partial \boldsymbol{x}_j$ material derivative with respect to $\boldsymbol{x}_j$ and the time t_i
$\mathrm{D}_{-\boldsymbol{u}_0,\boldsymbol{x}_m}$	=	$-i\omega - \boldsymbol{u}_0 \cdot \partial/\partial \boldsymbol{x}_m$ material derivative at the observer position written in the frequency domain
$F,\ f$	=	dummy variable to define the Fourier transform convention
l_s	=	parameter to model the sound source intercorrelation introduced by Tam & Auriault [3]
$\mathcal{L}_0$	=	linear operator
$\mathcal{L}_0^\dagger$	=	adjoint linear operator associated to $\mathcal{L}_0$ for the canonical scalar product $<\,,\,>$
M_{ext}	=	$\lvert\boldsymbol{u}_{ext}\rvert/a_\infty$ exterior medium Mach number
M_j	=	Mach number in the potential core of the jet
$\boldsymbol{M}_0$	=	$\boldsymbol{u}_0/a_0$ vectorial Mach number
$\boldsymbol{M}_{0,S}$	=	vectorial Mach number evaluated at the source position
M_∞	=	$\lvert\boldsymbol{u}_0\rvert/a_\infty$ acoustic Mach number
p	=	fluctuating pressure field

*Postdoctoral Fellow, Fluid Mechanics and Acoustics Laboratory (LMFA).
†Professor, Fluid Mechanics and Acoustics Laboratory (LMFA), AIAA Senior member.
‡Aeroacoustic Development Leader & Senior Research Engineer.

$p^\dagger$	=	adjoint field associated to p for the canonical scalar product $< , >$
$p^\dagger_{\boldsymbol{x}_m,t_m}$	=	adjoint Green's function associated to p for the adjoint source position $\boldsymbol{x}_m$ and time t_m
p_0	=	mean pressure field
$p_{C,0}$	=	customised mean pressure field provided as entry of *Actran TM*
Q	=	$\mathrm{D}(q_s)/\mathrm{D}t$ material derivative of q_s
q_s	=	sound source of Tam & Auriault's mixing noise model
$\hat{q}_s$	=	parameter to model the sound source intercorrelation introduced by Tam & Auriault [3]
$\boldsymbol{r}$	=	$\boldsymbol{x}_1 - \boldsymbol{x}_2$ space-separation used in the noise source intercorrelation model
$\boldsymbol{r}_\perp$	=	projection of $\boldsymbol{r}$ orthogonal to $\boldsymbol{u}_0$
R_{pp}	=	time-domain pressure autocorrelation
R_{QQ}	=	the space-time intercorrelation of the quantity Q
S_{pp}	=	Fourier transformed pressure autocorrelation
$\boldsymbol{S_u}$, S_p	=	generic writing of sound sources of $\mathcal{L}_0$
S_m	=	linearised momentum source potential
S, S_m, $\boldsymbol{S}_d$	=	generic writing of sound sources for normalised Möhring's equation
$\boldsymbol{S}^\dagger$	=	$\left(S^\dagger_{\rho_0 u_1^\dagger}, S^\dagger_{\rho_0 u_2^\dagger}, S^\dagger_{\rho_0 u_3^\dagger}, S^\dagger_{p^\dagger}\right)^T$ generic writing of the adjoint source term of $\mathcal{L}_0^\dagger$
St	=	Strouhal number
$St^o_{\max}$, $St^c_{\max}$	=	optimistic and conservative estimation of the Strouhal number cut-off limit of the grid
t, t_1, t_2	=	dummy time variable
t_m	=	microphone time, also corresponding to the adjoint source time
$\boldsymbol{u}$	=	fluctuating velocity field
$\boldsymbol{u}^\dagger$	=	adjoint field associated to $\boldsymbol{u}$ for the canonical scalar product $< , >$
$\boldsymbol{u}^\dagger_{\boldsymbol{x}_m,t_m}$	=	adjoint Green's function associated to $\boldsymbol{u}$ for the adjoint source position $\boldsymbol{x}_m$ and time t_m
$\boldsymbol{u}_{ext}$	=	exterior medium mean velocity field
$\boldsymbol{u}_0$	=	mean velocity field
$\boldsymbol{u}_{C,0}$	=	customised mean velocity field provided as entry of *Actran TM*
u_j	=	mean velocity in the potential core of a jet
$\boldsymbol{x}$, $\boldsymbol{x}_1$, $\boldsymbol{x}_2$	=	dummy space variable
$\boldsymbol{x}_m$	=	microphone position, also corresponding to the adjoint source position
$\boldsymbol{x}_{m,\perp}$	=	projection of $\boldsymbol{x}_m$ orthogonal to $\boldsymbol{u}_0$
$\boldsymbol{x}_s$	=	source position
α, β	=	intermediate calculation variable
γ	=	adiabatic index
$\delta_{\boldsymbol{x}_m,t_m}$	=	$\delta(\boldsymbol{x}-\boldsymbol{x}_m)\delta(t-t_m)$ delta Dirac function for the microphone position $\boldsymbol{x}_m$ and time t_m
$\delta_{\boldsymbol{x}_s}$	=	$\delta(\boldsymbol{x}-\boldsymbol{x}_s)$ delta Dirac function for the source position $\boldsymbol{x}_s$
Δt	=	$t_1 - t_2$ time-difference used in the noise source intercorrelation model
θ_m	=	jet polar angle
λ	=	acoustic wavelength
ρ_0	=	mean density field
$\rho_{T,0}$	=	total mean density
$\rho_{C,0}$	=	customised mean density field provided as entry of *Actran TM*
σ	=	standard deviation of the Gaussian velocity profile
σ_s	=	standard deviation of the Gaussian source distribution used in the in-house code
τ	=	time-shift
τ_s	=	parameter to model the sound source intercorrelation introduced by Tam & Auriault [3]
ϕ	=	acoustic potential solution of Pierce's equation
$\phi^\dagger$	=	adjoint field associated to ϕ for the canonical scalar product $< , >$
$\phi^\dagger_{\boldsymbol{x}_m,t_m}$	=	adjoint Green's function associated to ϕ for the adjoint source position $\boldsymbol{x}_m$ and time t_m
ω	=	acoustic pulsation

II. Introduction

When jet noise predictions are based on an acoustic analogy, the source statistics are usually modelled from a RANS computation [3–5]. The propagation of sound to the observer is then achieved analytically using Green's function and a simplified flow model. This strategy is computationally less demanding than a direct noise computation, but often fails to correctly predict the acoustic propagation effects in complex configurations like those encountered for installed modern aircraft engines. With a smart use of the reciprocity principle, Tam & Auriault [1] introduced the adjoint method and enabled the tackling of propagation effects in complex environments, for which analytical Green's functions are unknown. In the aeroacoustic community adjoint Green's functions are usually sought as a solution to a scattering problem, and as such, are ill-posed to properly account for the surface refraction and edge diffraction phenomena. In numerous applications, the effects of the latter are however predominant [6]. The present contribution proposes a numerical method able to deal with the presence of surfaces in the computation of adjoint Green's functions. The commercial software *Actran TM* is used for that purpose. RANS based mixing noise predictions are often conducted with Tam & Auriault's model [3] that is detailed in the following section. The acoustic propagation equations considered by these authors are derived from the linearised Euler equations, and also contain instability waves as a solution. Consequently, the method robustness is thereby regrettably deteriorated.

In this study, this mixing noise model is recast for the acoustic potential ϕ as computed with Pierce's equation so as to achieve an acoustic preserving formulation. Moreover because *Actran TM* solves the wave equation of Möhring's acoustic analogy [7], a reformulation of the mean flow fields provided in input of this software is proposed so to solve Pierce's equation. Finally, based on the flow reversal theorem (FRT), which proved to be equivalent to the adjoint approach for self-adjoint operators [8], an adjoint computation are executed for a jet flow exhausting a duct. This study aims at providing indications on how this tool may be used in statistical jet noise predictions.

III. Tam & Auriault's mixing noise model

In a well-known contribution, Tam *et al.* [9] gave experimental evidences for a separation in the mixing noise process of a jet foreseen by Ribner [10]. From this theory, two contributions arise in the noise caused by turbulent mixing; the first one is associated with the large-scales of the turbulence and second one finds its origin in the fine-scales. The mixing noise model of concern in this note is given by Tam & Auriault [3], and intends to model the sound radiated by the turbulence fine-scales. Since Lighthill's pioneer study [11] laying out the basis for all acoustic analogies that would follow, it is admitted that jet mixing noise is driven by the unsteadiness of the Reynolds stress tensor. A Fourier filtering is considered by Tam & Auriault to remove the large-scales present in this sound source, and is noted in the following with an overbar. In their model, the noise source is then identified with the trace of the filtered Reynolds stress tensor. These terms account for the fluid dilatation and compression. Based on the Boussinesq eddy viscosity model this source of sound can be directly related to the kinetic energy of the fine-scale turbulence per unit mass. An *isotropic* contribution of the modelled sound source q_s in the linearised momentum equation is then assumed. Hence, the direct problem for Tam & Auriault's mixing noise writes,

$$\begin{cases} \rho_0 \dfrac{\mathrm{D}(\boldsymbol{u})}{\mathrm{D}t} + \nabla p = -\nabla q_s \ , \\[2ex] \dfrac{\mathrm{D}(p)}{\mathrm{D}t} + \gamma p_0 (\nabla \cdot \boldsymbol{u}) = 0 \ , \end{cases} \tag{1}$$

and can be recast by defining the associated linear operator $\mathcal{L}_0$ into

$$\mathcal{L}_0 \begin{pmatrix} \boldsymbol{u} \\ p \end{pmatrix} = \begin{pmatrix} -\nabla q_s \\ 0 \end{pmatrix} , \tag{2}$$

where $\mathrm{D}/\mathrm{D}t = \partial/\partial t + \boldsymbol{u}_0 \cdot \nabla$ is the material derivative along the mean flow, ρ_0, $\boldsymbol{u}_0$, p_0 are the mean flow fields and $\boldsymbol{u}$, p the fluctuating ones. $\mathcal{L}_0$ corresponds to the linearised Euler's equations expressed for a parallel mean flow.

A. Governing adjoint equations

The governing adjoint equations are given by the Lagrange identity,

$$< \begin{pmatrix} \boldsymbol{u}^\dagger \\ p^\dagger \end{pmatrix}, \mathcal{L}_0 \begin{pmatrix} \boldsymbol{u} \\ p \end{pmatrix} > = < \mathcal{L}_0^\dagger \begin{pmatrix} \boldsymbol{u}^\dagger \\ p^\dagger \end{pmatrix}, \begin{pmatrix} \boldsymbol{u} \\ p \end{pmatrix} > \ . \tag{3}$$

Accordingly to Tam & Auriault's model [3], the free-space propagation problem will be considered, for which all boundary conditions vanish for the direct problem as well as for the adjoint problem. In particular the radiating boundary conditions associated to the previously introduced direct problem and their associated anti-causal adjoint boundary conditions, will be discarded. Multiple integrations by parts, and taking benefit from the mean flow parallelism, subsequent adjoint operator $\mathcal{L}_0^\dagger$ is obtained,

$$\begin{cases} -\rho_0 \dfrac{\mathrm{D}(\boldsymbol{u}^\dagger)}{\mathrm{D}t} - \gamma p_0 \nabla p^\dagger = \boldsymbol{S}^\dagger_{\rho_0 \boldsymbol{u}^\dagger} \ , \\ \\ -\dfrac{\mathrm{D}(p^\dagger)}{\mathrm{D}t} - \nabla \cdot \boldsymbol{u}^\dagger = S^\dagger_{p^\dagger} \ , \end{cases} \tag{4}$$

where $\boldsymbol{S}^\dagger = \left(S^\dagger_{\rho_0 u_1^\dagger}, S^\dagger_{\rho_0 u_2^\dagger}, S^\dagger_{\rho_0 u_3^\dagger}, S^\dagger_{p^\dagger}\right)^T$ is a generic writing of the adjoint source term. Because Tam & Auriault's model intends to compute the pressure field autocorrelation S_{pp} at a microphone position $\boldsymbol{x}_m$, a Dirac source term $\delta_{\boldsymbol{x}_m, t_m} \equiv \delta(\boldsymbol{x} - \boldsymbol{x}_m)\delta(t - t_m)$, for dummy space and time variables $\boldsymbol{x}$ and t in the equation governing the adjoint field associated with the pressure $p^\dagger$ is considered. Since an impulse response is considered, it follows that the corresponding adjoint fields $\boldsymbol{u}^\dagger$ and $p^\dagger$ are Green's functions. To bear in mind the source position $\boldsymbol{x}_m$ and time t_m, this information will be specified in the notations of Green's functions, leading thus to the adjoint problem hereafter,

$$\mathcal{L}_0^\dagger \begin{pmatrix} \boldsymbol{u}^\dagger_{\boldsymbol{x}_m, t_m} \\ p^\dagger_{\boldsymbol{x}_m, t_m} \end{pmatrix} = \begin{pmatrix} \boldsymbol{0} \\ \delta_{\boldsymbol{x}_m, t_m} \end{pmatrix} . \tag{5}$$

When replaced in Lagrange's identity together with the direct problem source term, the representation formula, analogous to [3, eq. (21)], is readily obtained,

$$< \begin{pmatrix} \boldsymbol{u}^\dagger_{\boldsymbol{x}_m, t_m} \\ p^\dagger_{\boldsymbol{x}_m, t_m} \end{pmatrix}, \begin{pmatrix} -\nabla q_s \\ 0 \end{pmatrix} > = < \begin{pmatrix} \boldsymbol{0} \\ \delta_{\boldsymbol{x}_m, t_m} \end{pmatrix}, \begin{pmatrix} \boldsymbol{u} \\ p \end{pmatrix} > \ . \tag{6}$$

And finally with the property of the delta Dirac function, the following relation is obtained,

$$p(\boldsymbol{x}_m, t_m) = - < \boldsymbol{u}^\dagger_{\boldsymbol{x}_m, t_m}, \nabla q_s > \ . \tag{7}$$

Following Tam & Auriault's steps, using integration by parts and the governing equation for $p^\dagger$, previous RHS is then reformulated as,

$$- < \boldsymbol{u}^\dagger_{\boldsymbol{x}_m, t_m}, \nabla q_s > = < \nabla \cdot \boldsymbol{u}^\dagger_{\boldsymbol{x}_m, t_m}, q_s > = \ - < \frac{\mathrm{D}(p^\dagger_{\boldsymbol{x}_m, t_m})}{\mathrm{D}t}, q_s > = < p^\dagger_{\boldsymbol{x}_m, t_m}, \frac{\mathrm{D}(q_s)}{\mathrm{D}t} > , \tag{8}$$

where again, all the contour integrals have been omitted since they vanish in the free-field. Note that $<,>$ has been used above indifferently for different size of vectors without ambiguity because the canonical scalar product is considered. This procedure can be applied for any scalar product. Notice however that, as a step by step derivation would show, the latter needs to be adapted to each new couple of fields considered.

B. Calculation of the pressure autocorrelation

Let the time-autocorrelation R_{pp} of the pressure p for a time-shift τ at position $\boldsymbol{x}_m$ be defined as,

$$R_{pp}(\boldsymbol{x}_m, \tau) = \int_{\mathbb{R}} \mathrm{d}t_m \ p(\boldsymbol{x_m}, t_m) p(\boldsymbol{x_m}, t_m + \tau) \ , \tag{9}$$

then Tam & Auriault's expression for the autocorrelation [3, eq. (24)] is retrieved:

$$R_{pp}(\boldsymbol{x}_m, \tau) \quad = \int_{\mathbb{R}} \mathrm{d}t_m \ \left\langle p^\dagger_{\boldsymbol{x}_m, t_m}, \frac{\mathrm{D}(q_s)}{\mathrm{D}t} \right\rangle \left\langle p^\dagger_{\boldsymbol{x}_m, t_m + \tau}, \frac{\mathrm{D}(q_s)}{\mathrm{D}t} \right\rangle \ . \tag{10}$$

And the pressure time autocorrelation R_{pp}, simply expresses without assumptions as,

$$R_{pp}(\boldsymbol{x}_m, \tau) \ = \int_{\Omega} \mathrm{d}\boldsymbol{x}_1 \int_{\Omega} \mathrm{d}\boldsymbol{x}_2 \int_{\mathbb{R}} \mathrm{d}t_1 \int_{\mathbb{R}} \mathrm{d}t_2 \ \ p^\dagger_{\boldsymbol{x}_m}(\boldsymbol{x}_1, t_1) \, p^\dagger_{\boldsymbol{x}_m}(\boldsymbol{x}_2, t_2 - \tau) \, R_{QQ}(\boldsymbol{x}_1, \boldsymbol{x}_2, \Delta t) \ , \tag{11}$$

where $\Delta t = t_1 - t_2$ and $R_{QQ}(\boldsymbol{x}_1, \boldsymbol{x}_2, \Delta t)$ is the space-time intercorrelation of the quantity $Q \equiv \mathrm{D}(q_s)/\mathrm{D}t$,

$$R_{QQ}(\boldsymbol{x}_1, \boldsymbol{x}_2, \Delta t) = \int_{\mathbb{R}} \mathrm{d}t_m \; \frac{\mathrm{D}(q_s(\boldsymbol{x}_1, t_m + \Delta t))}{\mathrm{D}t_m} \frac{\mathrm{D}(q_s(\boldsymbol{x}_2, t_m))}{\mathrm{D}t_m} \; . \tag{12}$$

C. Modelling of the source autocorrelation term

The modelling of R_{QQ} cannot be further postponed since its expression is needed to perform analytically the time integrations over t_1 and t_2. The Q-quantity space-time autocorrelation model proposed by Tam & Auriault [3, eq. (27)] is shift-invariant, i.e. by defining $\boldsymbol{r} = \boldsymbol{x}_1 - \boldsymbol{x}_2$, then $R_{QQ}(\boldsymbol{x}_1, \boldsymbol{x}_2, \Delta t) \equiv R_{QQ}(\boldsymbol{r}, \Delta t)$, valid for homogeneous turbulence, and writes

$$R_{QQ}(\boldsymbol{r}, \Delta t) = \frac{\hat{q}_s^2}{c^2 \tau_s^2} \exp\left(-\frac{|\boldsymbol{r} \cdot \boldsymbol{u}_0|}{u_0^2 \tau_s} - \frac{\ln(2)}{l_s^2} \left(\boldsymbol{r} - \boldsymbol{u}_0 \Delta t \right)^2 \right) , \tag{13}$$

The reader may refer to the original contribution of Tam & Auriault [3] for the definition of the above other variables and their origin. In our applications the Fourier transformed pressure autocorrelation S_{pp} is of interest and is defined as,

$$S_{pp}(\boldsymbol{x}_m, \omega) = \int_{\mathbb{R}} \mathrm{d}\tau \; R_{pp}(\boldsymbol{x}_m, \tau) e^{i\omega\tau} \; , \tag{14}$$

where $\alpha = \dfrac{l_s^2}{4\ln(2) u_0^2}$ and $\beta = \dfrac{\hat{q}_s^2 l_s}{c^2 \tau_s^2 u_0} \sqrt{\dfrac{\pi}{\ln(2)}}$. Fourier transforms are defined presently with,

$$F(\boldsymbol{x}, \omega) = \int_{\mathbb{R}} \mathrm{d}t \; f(\boldsymbol{x}, t) e^{i\omega t} \qquad \text{and,} \qquad f(\boldsymbol{x}, t) = \frac{1}{2\pi} \int_{\mathbb{R}} \mathrm{d}\omega \; F(\boldsymbol{x}, \omega) e^{-i\omega t} \; . \tag{15}$$

Several change of variables, Fourier transforms, other integral manipulations, and defining $\boldsymbol{r}_\perp = \boldsymbol{r} - (\boldsymbol{r} \cdot \boldsymbol{u}_0)\boldsymbol{u}_0/u_0^2$, lead to Tam & Auriault's equation (33) [3], with $u_0 = |\boldsymbol{u}_0|$,

$$S_{pp}(\boldsymbol{x}_m, \omega) = \int_\Omega \mathrm{d}\boldsymbol{x}_2 \int_\Omega \mathrm{d}\boldsymbol{r} \; \beta \, p^{\dagger}_{\boldsymbol{x}_m}(\boldsymbol{r} + \boldsymbol{x}_2, \omega) \, p^{\dagger}_{\boldsymbol{x}_m}(\boldsymbol{x}_2, \omega)^* \exp\left(-\frac{|\boldsymbol{r} \cdot \boldsymbol{u}_0|}{u_0^2 \tau_s} - \frac{\ln(2) |\boldsymbol{r}_\perp|^2}{l_s^2} - i\omega \frac{\boldsymbol{r} \cdot \boldsymbol{u}_0}{u_0^2} - \alpha\omega^2 \right) . \tag{16}$$

D. Approximated calculation of the double space integration

In the previous section, the double space integral defined by equation (16) is numerically unaffordable and a simplification is required. Two different simplifications are proposed hereafter.

1. Fraunhofer approximation

Because in Tam & Auriault's work the observer is set in the acoustic far field, those authors proposed to model two neighbour acoustic ray paths from the source region by a Fraunhofer-like approximation [3, fig. 4, eq. (34)], which expresses with vector notations as,

$$p^{\dagger}_{\boldsymbol{x}_m}(\boldsymbol{r} + \boldsymbol{x}_2, \omega) \approx p^{\dagger}_{\boldsymbol{x}_m}(\boldsymbol{x}_2, \omega) \exp\left(\frac{i\omega \, \boldsymbol{x}_m \cdot \boldsymbol{r}}{a_\infty |\boldsymbol{x}_m|} \right) , \tag{17}$$

where a_∞ is the ambient speed of sound. Note that this expression differs from the one proposed in the literature by the phase shift sign [3]. By defining $\boldsymbol{x}_{m,\perp} = \boldsymbol{x}_m - (\boldsymbol{x}_m \cdot \boldsymbol{u}_0)\boldsymbol{u}_0/u_0^2$, and replacing this formula in the expression of S_{pp}, the double integral simplifies into,

$$S_{pp}(\boldsymbol{x}_m, \omega) = \int_\Omega \mathrm{d}\boldsymbol{x}_2 \; \frac{2\hat{q}_s^2 l_s^3}{c^2 \tau_s} \left(\frac{\pi}{\ln(2)} \right)^{3/2} \left| p^{\dagger}_{\boldsymbol{x}_m}(\boldsymbol{x}_2, \omega) \right|^2 \frac{\exp\left(\dfrac{-\omega^2 l_s^2}{4\ln(2) u_0^2} \left(1 + \dfrac{u_0^2 |\boldsymbol{x}_{m,\perp}|^2}{a_\infty^2 |\boldsymbol{x}_m|^2} \right) \right)}{1 + \omega^2 \tau_s^2 \left(1 - \dfrac{\boldsymbol{u}_0 \cdot \boldsymbol{x}_m}{a_\infty |\boldsymbol{x}_m|} \right)^2} , \tag{18}$$

which is Tam & Auriault's fine-scale mixing noise formula [3, eq. (35)]. Note that above expression differs from the original one by a factor of 2π, which is related to different Green's function definition, refer to [3, eq. (19)], from which a $4\pi^2$ factor appears; then because of differences in the Fourier transform conventions, see [3, eq. (25)], the present relation should be divided by 2π to comply with Tam & Auriault's relation. Note furthermore that expression (18) is slightly enhanced compared to the original one, since it can address three dimensional propagation problems.

2. Taylor expansion

As suggested by Lielens [12], if adjoint Green's function $p^{\dagger}_{\boldsymbol{x}_m}$ is computed numerically for a near-field propagation problem, the knowledge of its spatial evolution can be capitalised and the Fraunhofer approximation can be replaced by a Taylor expansion; this paragraph presents the corresponding formula. If $\boldsymbol{r} = \boldsymbol{x}_1 - \boldsymbol{x}_2$ is small $p^{\dagger}{}^{(\boldsymbol{r}+\boldsymbol{x}_2,\omega)}_{\boldsymbol{x}_m}$ can be approximated by the first order Taylor expansion,

$$p^{\dagger}{}^{(\boldsymbol{r}+\boldsymbol{x}_2,\omega)}_{\boldsymbol{x}_m} \approx p^{\dagger}{}^{(\boldsymbol{x}_2,\omega)}_{\boldsymbol{x}_m} + \boldsymbol{r}\cdot\frac{\partial p^{\dagger}{}^{(\boldsymbol{x}_2,\omega)}_{\boldsymbol{x}_m}}{\partial \boldsymbol{x}_2} \ . \tag{19}$$

Replacing this expression in the formula for S_{pp} leads to following expression for the pressure autocorrelation,

$$S_{pp}(\boldsymbol{x}_m,\omega) = \int_{\Omega}\mathrm{d}\boldsymbol{x}_2\ \frac{2\hat{q}_s^2 l_s^3}{c^2\tau_s}\left(\frac{\pi}{\ln(2)}\right)^{3/2} p^{\dagger}{}^{(\boldsymbol{x}_2,\omega)^*}_{\boldsymbol{x}_m}\ \frac{\exp\left(-\dfrac{\omega^2 l_s^2}{4\ln(2)u_0^2}\right)}{1+\omega^2\tau_s^2}\left(p^{\dagger}{}^{(\boldsymbol{x}_2,\omega)}_{\boldsymbol{x}_m} - \frac{2i\omega\tau_s^2}{1+\omega^2\tau_s^2}\left(\boldsymbol{u}_0\cdot\frac{\partial p^{\dagger}{}^{(\boldsymbol{x}_2,\omega)}_{\boldsymbol{x}_m}}{\partial \boldsymbol{x}_2}\right)\right) \ . \tag{20}$$

IV. Tam & Auriault's formula applied to Pierce's wave equation

Tam & Auriault's formula [3, eq. (35)] relies on the prior computation of adjoint Green's function $p^{\dagger}_{\boldsymbol{x}_m}$ recalled by the above set of equations. This presents two limitations for the practical use of this theory; firstly efficient solvers that can simultaneously compute these equations and handle complex geometries are scarce, and secondly as for the direct problem, these equations do also present physical unstable modes. A reformulation of Tam & Auriault's formula for a propagation operator based on Pierce's equation [2, eq. (27)] is a way of overcoming these difficulties. The formulation proposed by Pierce based on the acoustic potential ϕ, defined by $\rho_0\boldsymbol{u} = \nabla\phi$ and thus $p = -\mathrm{D}\phi/\mathrm{D}t$, is indeed energy preserving and solvers, e.g. *Actran TM* can be configured to solve this wave equation.

The acoustic analogy based on Pierce's wave equation writes

$$\frac{\mathrm{D}^2(\phi)}{\mathrm{D}t^2} - \nabla\cdot(a_0^2\nabla\phi) = \frac{\mathrm{D}(S_m)}{\mathrm{D}t} - S_p \ , \tag{21}$$

and,

$$\Delta S_m = \nabla\cdot(\rho_0 \boldsymbol{S_u}) \ , \tag{22}$$

where ($\boldsymbol{S_u}$,S_p) is the general writing of a source term for the linearised momentum and energy equations. Because Pierce's wave equation describes solely the propagation of potential acoustic fluctuations ϕ, the source term for this equation needs to be potential as well. This is the meaning of the introduction of the linearised momentum source potential S_m. From the source model for mixing noise of Tam & Auriault's, it comes directly that $S_m = -q_s$ and $S_p = 0$.

A. Pressure autocorrelation with an acoustic potential description

Pierce's wave equation is self-adjoint for the canonical scalar product, and its adjoint Green's function is defined by,

$$\frac{\mathrm{D}^2(\phi^{\dagger}_{\boldsymbol{x}_m,t_m})}{\mathrm{D}t^2} - \nabla\cdot(a_0^2\nabla\phi^{\dagger}_{\boldsymbol{x}_m,t_m}) = \delta_{\boldsymbol{x}_m,t_m} \ . \tag{23}$$

The application of Lagrange's identity then gives,

$$\phi(\boldsymbol{x}_m,t_m) = <\phi^{\dagger}_{\boldsymbol{x}_m,t_m}, -\frac{\mathrm{D}(q_s)}{\mathrm{D}t}> \ . \tag{24}$$

The pressure time autocorrelation is hence defined by,

$$R_{pp}(\boldsymbol{x}_m,\tau) = \int_{\mathbb{R}}\mathrm{d}t_m\ p(\boldsymbol{x}_m,t_m)p(\boldsymbol{x}_m,t_m+\tau) = \int_{\mathbb{R}}\mathrm{d}t_m\ \frac{\mathrm{D}(\phi)}{\mathrm{D}_{t_m,\boldsymbol{x}_m}}\frac{\mathrm{D}(\phi)}{\mathrm{D}_{t_m+\tau,\boldsymbol{x}_m}} \ , \tag{25}$$

where $\mathrm{D}/\mathrm{D}_{t_i,\boldsymbol{x}_j} = \partial/\partial t_i + \boldsymbol{u}_0\cdot\partial/\partial\boldsymbol{x}_j$ is the material derivative with respect to $\boldsymbol{x}_j$ and the reference time t_i.

B. Far-field prediction formula with wind

After some algebra [13] very similar to those performed by Tam & Auriault [3], and with the same source model, the prediction formula expresses in the far-field, i.e. owning on a Fraunhofer approximation, as

$$S_{pp}(\boldsymbol{x}_m,\omega) = \int_\Omega \mathrm{d}\boldsymbol{x}_2 \; \frac{2\hat{q}_s^2 l_s^3}{c^2\tau_s}\left(\frac{\pi}{\ln(2)}\right)^{3/2}\left|\mathrm{D}_{-\boldsymbol{u}_0,\boldsymbol{x}_m}\left(\phi^{\dagger}{}^{(\boldsymbol{x}_2,\,\omega)}_{\boldsymbol{x}_m}\right)\right|^2 \frac{\exp\left(\dfrac{-\omega^2 l_s^2}{4\ln(2)u_0^2}\left(1+\dfrac{u_0^2|\boldsymbol{x}_{m,\perp}|^2}{a_\infty^2|\boldsymbol{x}_m|^2}\right)\right)}{1+\omega^2\tau_s^2\left(1-\dfrac{\boldsymbol{u}_0\cdot\boldsymbol{x}_m}{a_\infty|\boldsymbol{x}_m|}\right)^2}\,, \qquad (26)$$

where $\mathrm{D}_{-\boldsymbol{u}_0,\boldsymbol{x}_m} = -i\omega - \boldsymbol{u}_0\cdot\partial/\partial\boldsymbol{x}_m$ is the material derivative at the observer location written in the frequency domain with reversed flow. For a far-field observer $\boldsymbol{x}_m$ and with a constant free-stream wind as depicted in figure 1, the expression of this material derivative can be computed analytically. It is worth noticing that the adjoint field $\phi^{\dagger}_{\boldsymbol{x}_m}$

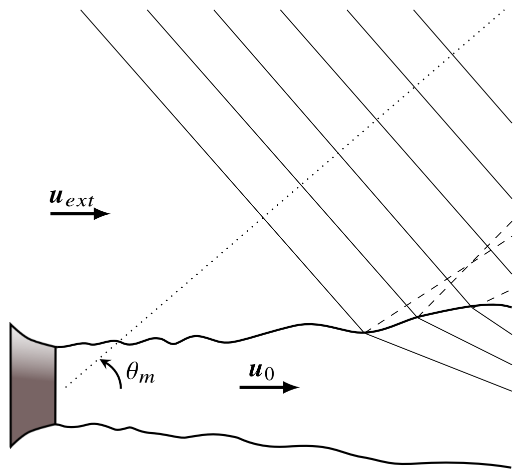

Fig. 1 When the microphone is in the acoustic far field, the polar angle θ_m is enough to characterise the adjoint function of a round jet.

is anti-causal and travels outward of the domain. Neglecting the azimuthal dependence, the mixing noise prediction formula in presence of wind writes,

$$S_{pp}(\theta_m,\omega) = \int_\Omega \mathrm{d}\boldsymbol{x}_2 \; \frac{2\omega^2\hat{q}_s^2 l_s^3}{c^2\tau_s}\left(\frac{\pi}{\ln(2)}\right)^{3/2}\left|\phi^{\dagger}{}^{(\boldsymbol{x}_2,\,\omega)}_{\theta_m}\right|^2\left(1+\frac{M_{ext}\cos\theta_m}{1+M_{ext}\cos\theta_m}\right)^2 \frac{\exp\left(\dfrac{-\omega^2 l_s^2}{4\ln(2)u_0^2}\left(1+M_\infty^2\sin^2\theta_m\right)\right)}{1+\omega^2\tau_s^2\left(1-M_\infty\cos\theta_m\right)^2}\,, \quad (27)$$

where $M_\infty = |\boldsymbol{u}_0|/a_\infty$ and $M_{ext} = |\boldsymbol{u}_{ext}|/a_\infty$ and with the adjoint source, i.e. the microphone, set in the far-field, that is $\phi^{\dagger}{}^{(\boldsymbol{x}_2,\,\omega)}_{\boldsymbol{x}_m} \to \phi^{\dagger}{}^{(\boldsymbol{x}_2,\,\omega)}_{\theta_m}$, where θ_m is the jet polar angle as defined in figure 1.

V. Computing adjoint Green's function $\phi^{\dagger}_{\boldsymbol{x}_m}$ with *Actran TM*

A recent investigation by the authors [8] has shown that adjoint solutions to propagation problems could be computed equivalently for self-adjoint operators with the so-called flow reversal theorem (FRT). The FRT states that the reciprocal acoustic solution over a moving flow can be obtained by simply reversing the direction of the flow. A procedure for Pierce's equation is here proposed, using the commercial software *Actran TM*.

A. Fundamental wave equation solved in *Actran TM*

Actran TM is a finite element code written in the frequency domain capable of handling complex geometries. Möhring's equation written for the normalised fluctuating stagnation enthalpy b is solved,

$$\frac{\partial}{\partial t}\left[\frac{\rho_0}{\rho_{T,0}^2 a_0^2}\frac{\mathrm{D}b}{\mathrm{D}t}\right] + \nabla\cdot\left[\frac{\rho_0\boldsymbol{u}_0}{\rho_{T,0}^2 a_0^2}\frac{\mathrm{D}b}{\mathrm{D}t} - \frac{\rho_0}{\rho_{T,0}^2}\nabla b\right] = \quad S\,, \qquad (28)$$

where $\mathrm{d}b = \rho_{T,0}\mathrm{d}B$, and B is the usual total enthalpy. By introducing the Mach number $\boldsymbol{M}_0 = \boldsymbol{u}_0/a_0$, the total mean density $\rho_{T,0}$, expresses as,

$$\rho_{T,0} = \rho_0 \left(1 + \frac{\gamma - 1}{2}\boldsymbol{M}_0^2\right)^{1/(\gamma-1)} . \tag{29}$$

It can be observed that equation (28) is linear, in contrast to the original equation proposed by Möhring [7]. Generic monopole S_m and dipole $\boldsymbol{S}_d$ source terms are considered in the software for equation (28).

$$S = \frac{\partial S_m}{\partial t} + \nabla \cdot \boldsymbol{S}_d . \tag{30}$$

Finally, the pressure field is calculated from the relationship,

$$\frac{\rho_{T,0}}{\rho_0}\frac{\partial p}{\partial t} = \frac{\mathrm{D}b}{\mathrm{D}t} . \tag{31}$$

B. Solving Pierce's equation with *Actran TM*

A key remark at this step is that Pierce's wave equation (21) can be obtained from equation (28) solved by *Actran TM* by setting $\rho_{T,0} = \rho_0$ and by identifying the normalised enthalpy b with the acoustic potential ϕ. In this software, it is not possible however to force the equality $\rho_{T,0} = \rho_0$. The expression of the mean stagnation density $\rho_{T,0}$ is indeed directly computed from the mean density ρ_0 and the mean Mach number $\boldsymbol{M}_0$ inside the solver. This hardship is overcome by preprocessing the mean flow fields ρ_0, p_0 and $\boldsymbol{u}_0$ given in input, so to compensate in the solved equation the presence of the total mean density $\rho_{T,0}$. The source amplitude needs to be corrected along with this transformation. Note that, if all the flow fields required for an analysis are not provided by the user, *Actran TM* will rebuilt them from the fields given in input. If this is not possible, default values are used in the computation. The input fields must be defined in a consistent way, and redundancy may be a good practise to ensure this.

1. Preprocessing of the mean flow given in input

The goal is to solve Pierce's equation for the physically relevant mean flow fields ρ_0, p_0 and $\boldsymbol{u}_0$. To achieve this, some customised mean flow fields are defined and provided as entries for *Actran TM*. Let these customised variables be renamed by adding a C in subscript as $\rho_{0,C}$, $p_{0,C}$, $\boldsymbol{u}_{0,C}$ and $a_{0,C}$. An inspection of *Actran TM*'s equation and Pierce's one indicates that subsequent transformations need to be achieved to turn Möhring's equation of *Actran TM* into Pierce's wave equation,

$$\boldsymbol{u}_{0,C} = \boldsymbol{u}_0 , \qquad a_{0,C} = a_0 , \text{ and } \qquad \frac{\rho_{0,C}}{\rho_{T,0}^2} = \frac{1}{\rho_0} . \tag{32}$$

It comes out, that the mean velocities $\boldsymbol{u}_0$ and a_0 are not affected by these transformations. Because in general $\rho_{C,0} \neq \rho_0$, equation (29) cannot be used in this transformation and needs to be replaced by,

$$\rho_{T,0} = \rho_{0,C} \left(1 + \frac{\gamma - 1}{2}\frac{\rho_{0,C}}{\gamma p_{0,C}}\boldsymbol{u}_{0,C}^2\right)^{1/(\gamma-1)} . \tag{33}$$

Because the mean density ρ_0 is corrected, for $a_0 = \sqrt{\gamma p_0/\rho_0} = \sqrt{\gamma p_{0,C}/\rho_{0,C}}$ to remain unchanged in the transformation, the mean pressure $p_{0,C}$ given in entry of *Actran TM* needs to be modified as well. Finally, to solve Pierce's equation with this software, the pre-processing adjustments that need to be done on $\rho_{0,C}$ and $p_{0,C}$ reads,

$$\frac{p_{0,C}}{p_0} = \frac{\rho_{0,C}}{\rho_0} = \left[1 + \frac{\gamma - 1}{2}\frac{\boldsymbol{u}_0^2}{a_0^2}\right]^{-2/(\gamma-1)} . \tag{34}$$

It must be mentioned, that to identically retrieve Pierce's equation from the relation (32) and equation (28), mean pressure gradients ∇p_0 have been neglected. This approximation is fully satisfied by open flows.

2. Correction of the source amplitude

In *Actran TM*, there are three kinds of source amplitude definitions, sources referred to as '*P*' type, '*Q*' type or '*V*' type (cf. keyword '*AMPLITUDE_TYPE*'). The type '*P*' amplitude is default and is related to the pressure field, while the '*Q*' type amplitude is related to the mass flow rate and the '*V*' type source is related to the volume source [14, § 28.4.3][15, § 9.50.3]. In the present study, a source amplitude of type '*P*' is considered. When the above preprocessing step is conducted to turn *Actran TM* into a Pierce's equation solver, the acoustic potential ϕ solution of Pierce's equation for a pointwise source in $\boldsymbol{x}_s$,

$$\frac{\mathrm{D}^2\phi}{\mathrm{D}t^2} - \nabla\cdot(a_0^2\nabla\phi) = A\ \delta_{\boldsymbol{x}_s}\ , \tag{35}$$

is related to the computed stagnation enthalpy b by,

$$\phi^* = \frac{-i\omega A}{4a_{0,S}^2}\left(1+\frac{\gamma-1}{2}\boldsymbol{M}_{0,S}^2\right)^{-1/(\gamma-1)} b\ , \tag{36}$$

for a bidimensional configuration. When a three-dimensional geometry is considered, the sound source is spherical instead of cylindrical and the acoustic potential ϕ is deduced from the stagnation enthalpy solved by *Actran TM* with,

$$\phi^* = \frac{-i\omega A}{4\pi a_{0,S}^2}\left(1+\frac{\gamma-1}{2}\boldsymbol{M}_{0,S}^2\right)^{-1/(\gamma-1)} b\ , \tag{37}$$

where ϕ^* is the complex conjugate of ϕ, A the complex source amplitude defined in the software, ω the investigated acoustic pulsation, $a_{0,S}$, and $\boldsymbol{M}_{0,S}$, the speed of sound and Mach number evaluated at the source position. This amplitude correction depends only on a_0 and M_0 and is therefore insensitive to the $\rho_{0,T}$ correction procedure.

C. Validation of *Actran TM*'s background mean flow fields reformulation

The ability of *Actran TM* to solve properly Pierce's equation over a sheared and stratified flow is verified for the Gaussian heated jet flow profile taken from the fourth CAA workshop [8, 16]. The sound field computed by this commercial software for a point source set in the flow region with a pulsation of $\omega = 200\pi$ rad $\cdot$ s^{-1}, is compared with the results obtained with a in-house finite difference code developed in the frequency domain [8]. *Actran TM*'s finite element formulation considers delta Dirac sources, while for the in-house finite difference solver, the source is voluminous by nature. A normalised Gaussian source distribution of standard deviation σ_s is chosen to approximate the delta Dirac sound source considered by *Actran TM* with the in-house code. Meshes considered by the in-house code are regular, two simulations with different source compactnesses are performed. The first configuration considers a source−wavelength ratio of $\lambda/\sigma_s \approx 23$, while for the second a finer but smaller domain achieves a ratio of $\lambda/\sigma_s \approx 1.4\times10^2$ (with identical number of grid points), that is deemed high enough to assume source compactness. In this validation, PML boundary conditions are considered for both solvers. Figure 2 shows the computed fields without the non reflecting layers, and figure 3 compares the horizontal extracts of the computed fields for $x_2/\sigma = 0.0$, $x_2/\sigma = 9.0$, where σ corresponds to the standard deviation of the Gaussian velocity profile. Comparable element size are considered for the in-house code with coarse mesh, and the *Actran TM* grid. Both solver require approximatively 5 points per wavelength to solve accurately sound propagation, see § V.D. On these two meshes, a wavelength in the quiescent region is resolved with 33 points and by $33\times(1-0.756)\approx 8$ points per wavelength in the jet flow region.

Figure 2 indicates an overall excellent qualitative agreement. Outside of the shadow zone where the acoustic amplitude is low, and apart from the source compactness issue discussed later on, these three fields coincide with a deviation of less than 2%. The small discrepancies are likely to correspond to acoustic reflection at NRBC. Upstream of the source, the computation with the less compact source slightly under-estimates the acoustic level obtained with the compact sources. This is most easily seen when the absolute part of the potential field ϕ is considered, see the extract along the jet axis in figure 3. It should be noted that this effect of the source non-compactness is reduced further away of the source, and the acoustic field obtained with the more broad source term can is comparable to the compact sound source solutions. It is seen indeed that the extracts along $x_2/\sigma = 9.0$ computed with the in-house code and corresponding to two different source compactness coincide.

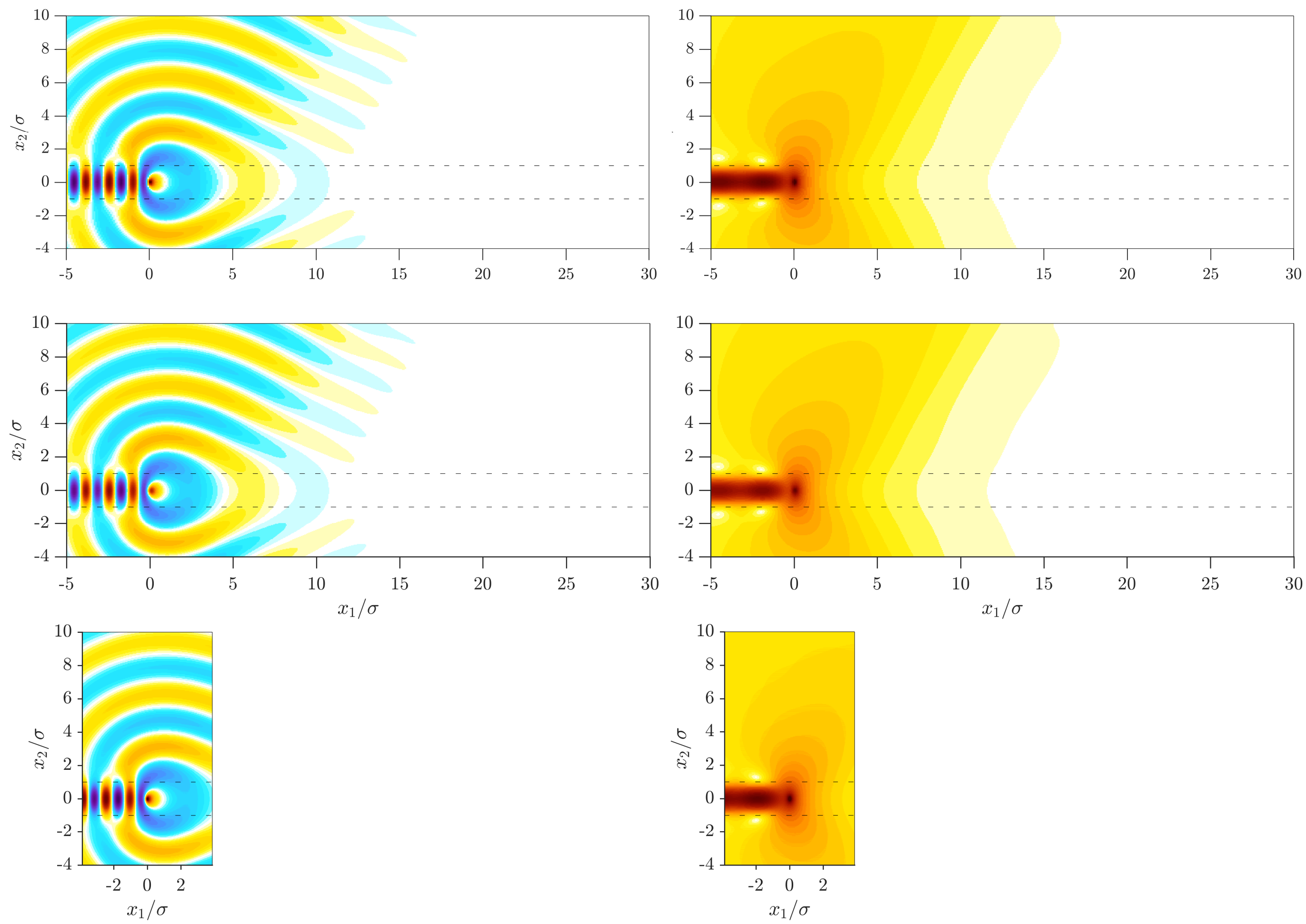

Fig. 2 Real part (left) and absolute part (right) of the acoustic potential ϕ obtained for a point source in a sheared and stratified flow. The fields are computed with *Actran TM* considering the background flow field reformulation (top) and the in-house code considering a sound source compactness of $\lambda/\sigma_s \approx 23$ (middle) and $\lambda/\sigma_s \approx 1.4 \times 10^2$ (bottom).

The computations achieved with the in-house code consider a regular structured domain of 800×450 requiring 43 GB of RAM. Whereas the resolution with *Actran TM* over a mesh of 430 000 nodes (215 000 quadratic two-dimensional unstructured elements), which has approximatively the size of mesh used in the other calculations, needs only 1.7 GB. Finite difference and finite element methods are fairly different techniques and a too strict comparison may not be fair, however PROPA and *Actran TM* with second order elements require both a minimum of 5 elements per wavelength to resolve acoustic travelling waves. This huge gain in computation cost, and the ability of *Actran TM* to consider complex geometries, represent tremendous advantages over the in-house code, when Pierce's equation has to be solved in realistic applications.

D. Choice of the numerical parameters

Actran TM offers a wide choice of parameters to configure the numerical setup. Some documentation on the HPC performance of *Actran TM* exist [17], this section investigates the mesh size requirements regarding the order of the finite elements considered, the benefit of considering single precision with respect to double precision is also discussed. The deviation from a solution field ϕ to a given reference solution ϕ_{ref} is measured with the euclidean norm ξ, defined

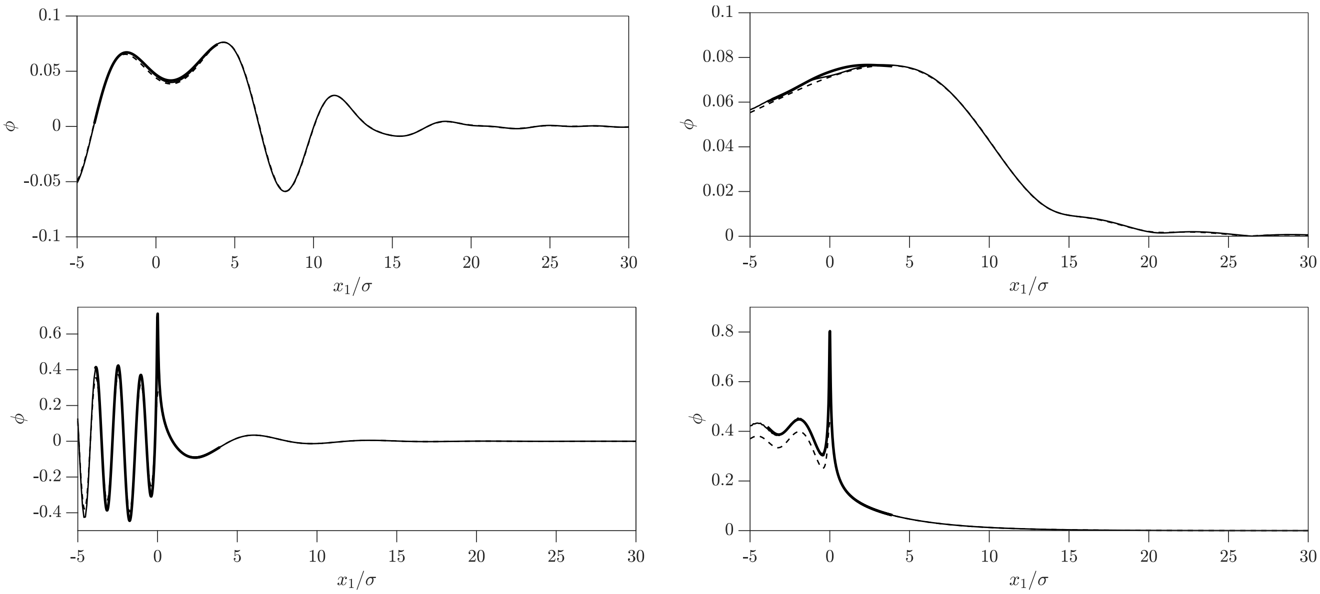

Fig. 3 Extracts along $x_2/\sigma = 9.0$ (top) and $x_2/\sigma = 0$ (bottom) of the real part of the acoustic potential ϕ (left) and its absolute part $|\phi|$ (right). Fields are computed with, —— *Actran TM* and, - - - the in-house code considering a source compactness of $\lambda/\sigma_s \approx 23$ and, ▬▬ $\lambda/\sigma_s \approx 1.4 \times 10^2$.

over a volume V by,

$$\xi(\phi, \phi_{ref}) = \sqrt{\frac{\int_V |\phi - \phi_{ref}|^2 \mathrm{d}V}{\int_V |\phi_{ref}|^2 \mathrm{d}V}} \,. \tag{38}$$

So as to come close to the jet exhaust configuration that is considered for the adjoint analysis presented in § VI.C, the domain considered is cylindrical, the source is spherical and set out of the computational domain as illustrated in figure 4. The angle of the sound source with respect to the cylinder axis is 30^o. The computational domain has a radii of 10Δ and extends over 40Δ, where Δ is the element size considered. the source is set at a distance of approximatively 100Δ from the domain. The mean flow is uniform and in line with the axis of the cylinder. Depending on the flow direction and the source angular position, the effective wavelength of the acoustic wavefront $\lambda_{\text{eff}} = \lambda(1 + M\cos(\theta))$ propagating over the mean flow is shorter or longer compared to the acoustic wavelength at rest λ, leading to favourable or unfavourable numerical conditions. Infinite elements [18] with an order of 20 are used to achieve non reflecting boundary conditions.

For this simple configuration, an analytical solution ϕ_{ref} described by equations (49) and (50) exist, and it is possible to compute a measure of the numerical error. Different Mach numbers M ranging from $M = -0.8$ to $M = 0.8$ are investigated to verify that the solver's accuracy scales with the effective wavelength λ_{eff}. Figure 4, right, presents the evolution of the error ξ for different grid point per wavelength ratio. The accuracy corresponding to quadratic and linear elements is presented. A fairly good collapse of the data is obtained for different Mach numbers M confirming the correctness and robustness of the scaling in $\lambda_{\text{eff}}/\Delta$. As expected for a given number of points per wavelength quadratic elements achieve better than linear ones. For the Euclidean norm considered, quadratic elements makes it possible to achieve an accuracy better than 1%, while linear elements have difficulties reaching it even with many points per wavelength. An abrupt slope discontinuity can be observed using quadratic elements showing only little benefit considering more than 5 points per wavelength. In the analysis performed here, quadratic elements are chosen and confidence in the computation is granted down to effective frequencies λ_{eff} of 5Δ.

The acoustic spectra of a simple round jet of diameter D_j with Mach number $M_j = 0.9$ is considered in the remaining part of this study, and it is convenient to introduce the Strouhal number St,

$$St = \frac{f\, D_j}{u_j} = \frac{D_j}{\lambda\, M_j} \,, \tag{39}$$

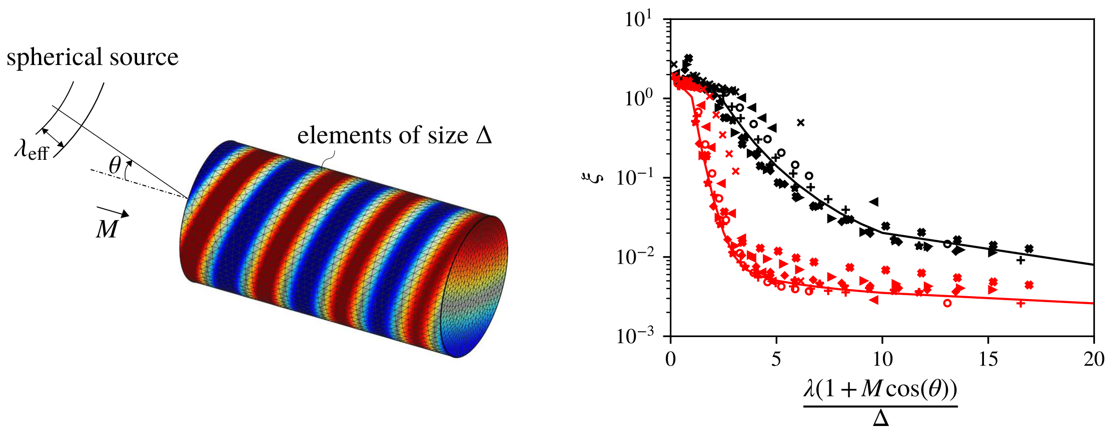

Fig. 4 Sketch of the numerical setup used to quantify the accuracy of the solver (left), and integrated error ξ computed over a range of points per wavelength ratio $\lambda_{\text{eff}}/\Delta$ (right), —— linear and, —— quadratic order elements are considered with $\theta = 30^o$. The lines correspond to the configuration without ambient flow. Flows with different Mach numbers are considered along the cylinder axis, ✕ $M = -0.8$ ◀ $M = -0.6$ ○ $M = -0.4$ ✚ $M = -0.2$ ★ $M = 0.2$ ◆ $M = 0.4$ ▶ $M = 0.6$ ✖ $M = 0.8$.

that is a normalisation of the frequency f by the jet velocity u_j. An unstructured mesh with a roughly uniform grid size of αD_j is considered. Before starting an aeroacoustic computation, it is necessary to know the mesh size required to calculate a target frequency with confidence. Since the variation of the jet mean velocities are strong by essence, the value of λ_{eff} that appears in the criteria $\lambda_{\text{eff}}/\Delta > 5$ significantly varies on the computational domain. Two grid cut-off Strouhal numbers are therefore computed, an optimistic one $St^o_{\max}$ considering the quiescent configuration and a conservative one $St^c_{\max}$ built on the highest jet velocity. Theses grid cut-off Strouhal numbers express as,

$$St^o_{\max} = \frac{1}{5\alpha M_j} \qquad \text{and,} \qquad St^c_{\max} = \frac{1 - M_j}{5\alpha M_j}\,. \tag{40}$$

It is immediately seen that a decade separates $St^o_{\max}$ from $St^c_{\max}$ when a Mach number of $M_j = 0.9$ is considered, making the conservative criterium hard to be fulfilled in three-dimensional high Mach number flow applications due to enormous computational needs.

The discrepancies between single precision and double precision representation of the floating points are then analysed. This is of interest, since frequency domain computations are greedy in RAM resources and that for an identical configuration, only half RAM memory is needed when single precision is used. A jet exhaust configuration similar to the one presented in § VI.C, with a grid size of $0.2D_j$ is considered for that investigation. The error ξ of a single precision solution $\phi_{32\text{bits}}$ measured with respect to a double precision solution $\phi_{64\text{bits}}$ is presented in figure 5 for the range of Strouhal of interest. It is seen that the integrated error ξ presents a plateau, with strong peaks however, from $St = 0.01$ to $St = 1$. After a hump the measure of the error ξ exponentially increases from $St = 1$ to $St = 10$. For this grid with element size of $0.2D_j$, the optimistic cut-off bound is $St^o_{\max} \sim 1.1$ and coincides with the increase of the error. It is likely that this steady increase in the deviation between double and single floating point representation corresponds to numerical noise that is amplified by the truncation error. From the asymptotic behaviour of the curve plotted in figure 5, it appears that the mesh cut-off Strouhal number most likely lies around $St \approx 1.0$ for this mesh. This is consistent with the value of $St^o_{\max}$ calculated for this mesh. On a sample of grid points computed for $St = 0.01$, it has been observed that $\phi_{32\text{bits}}$ deviates from $\phi_{64\text{bits}}$ by a digit at the third significant figure. ξ indicated that this error is roughly steady up to the optimistic limit of confidence of the mesh $St^o_{\max}$. This error is moreover fairly small and it is found advantageous to perform single precision computation to benefit from the reduction in RAM costs.

VI. Application to a $M_j = 0.9$ round jet

Tam & Auriault's model formulated for the acoustic potential is applied to a $M_j = 0.9$ round jet for which adjoint Green's functions are computed with *Actran TM*, and, hence are properly tailored to the jet flow exhausting from the

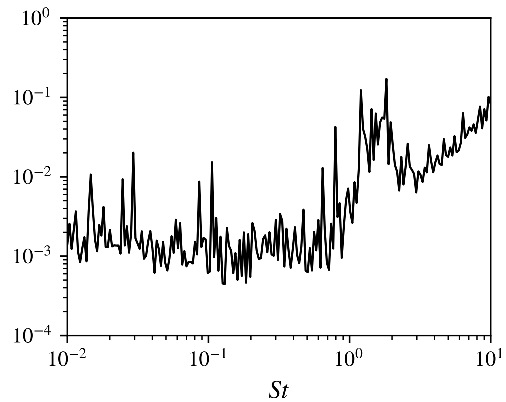

Fig. 5 Evolution of the error $\xi(\phi_{32\mathbf{bits}}, \phi_{64\mathbf{bits}})$ comparing the solution computed using single precision floating point operations $\phi_{32\mathbf{bits}}$ with the double precision solution $\phi_{64\mathbf{bits}}$. The fields $\phi_{32\mathbf{bits}}$ and $\phi_{64\mathbf{bits}}$ are solved for a jet exhaust configuration with element size of $0.2D_j$.

duct. The characteristic time τ_s and length scale l_s of Tam & Auriault's sound source model are calibrated with a high fidelity LES, and noise predictions are made perpendicular to the jet axis.

A. Numerical setup

The computational aeroacoustic grid corresponding to the exhaust of a high speed jet is created with *Actran*'s built-in meshing tools. The physical domain is composed by a duct of radius D_j and of length $5D_j$, from the duct end, the domain is $20D_j$ long and has a cylindrical shape whith a radius of $2.5D$. A fillet is applied at the edges of the cylinder to avoid numerical singularities at the corners. Both perfectly matched layer (PML) or with infinite elements (IE) are considered to achieve a truncation of the numerical domain. *Actran TM* does not enable the computation of an incident sound wave from a source set out of the computational domain when the frontier of the domain are mapped with a non-uniform flow. A $0.5D_j$ thick transition layer is therefore built to interface the physical domain and the non-reflecting boundary condition (NRBC). Figure 6 presents the numerical setup corresponding to a mesh with element size of $0.2D_j$ and a PML region with a width of $1.5D_j$. IE relies solely on a surface mesh and the exterior skin of the transition layer is used for that purpose. The mesh is composed by a combination of quadratic order tetrahedral and hexahedral elements. To improve numerical performances [19] and reduce the number of elements that are needed, hexahedral elements are used to generate the mesh with the *hexacore* option of *Actran*'s meshing tools.

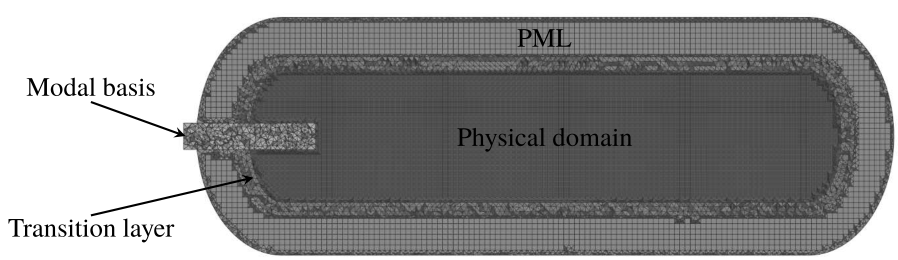

Fig. 6 Slice of the computational aeroacoustic grid using a PML to simulate free-field radiation.

The flow in the duct is uniform. By the decomposition of the acoustic wave on a modal basis, the duct is modelled as a semi-infinite tube. Figure 7 presents the Mach number and the turbulent kinetic energy mapped on the computational domain with elements of size $0.2D_j$. The mean velocity $\boldsymbol{u}_0$, mean pressure p_0 and mean density ρ_0 fields are smoothed to the ambient value before reaching the frontier of the domain. This smoothing is linear, and is applied for $x/D_j > 18$ and $r/D_j > 2$. It is visible on the Mach number field.

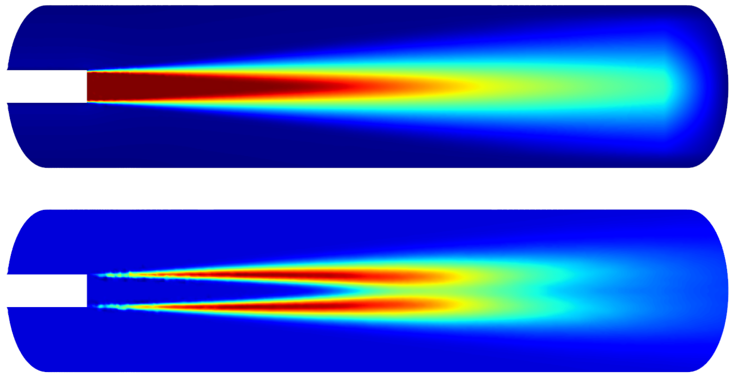

Fig. 7 Mach number M and turbulent kinetic energy k interpolated on the 'physical domain' subdomain.

The mesh generation process is scripted and grids with different element size are considered. Figure 8 presents a zoom of two meshes with element size of $0.1D_j$ and $0.2D_j$.

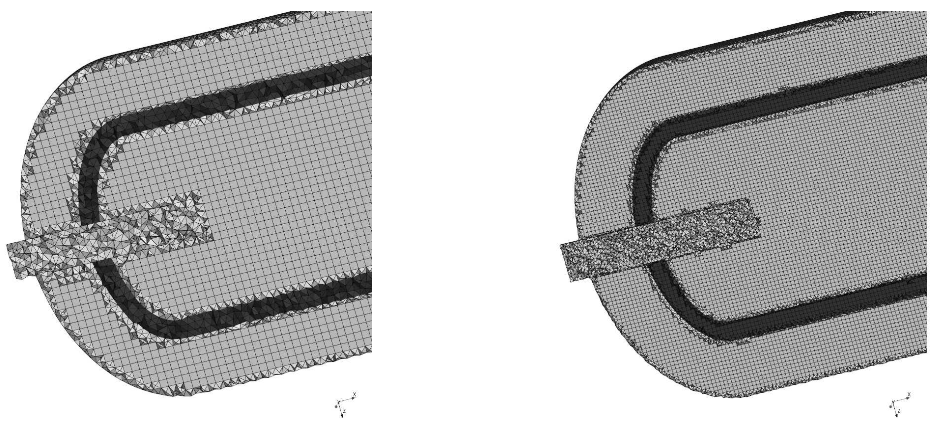

Fig. 8 Detail of the meshes with element size of $0.1D_j$ and $0.2D_j$ considered.

B. Parameters of the sound source

The mean flow and the turbulent kinetic energy k shown in figure 7 are obtained by averaging the solution of a high-fidelity LES [20, 21]. The mean velocity $\boldsymbol{u}_0$, mean density ρ_0 and mean pressure p_0 are used to model the acoustic refraction effects encountered in the jet. The background mean flow fields reformulation described in § V.B is applied on these averaged quantities prior to their usage in *Actran TM*, so to solve Pierce's equation. To enable the computation of adjoint Green's functions $\phi^{\dagger}_{\boldsymbol{x}_m}$, the flow reversal theorem (FRT) is also applied beforehand. In addition to this, these averaged fields, without any transformation, are needed to inform Tam & Auriault's mixing noise model.

From the sound source autocorrelation, equation 13, the three variables $\hat{q}_s/c$, τ_s and l_s, have to be modelled. Tam & Auriault proposed to model them with a k-ε flow solution [3] by defining,

$$l_s = c_l \frac{k^{3/2}}{\varepsilon} \ , \qquad \tau_s = c_\tau \frac{k}{\varepsilon} \ \text{and,} \ \ \frac{\hat{q}_s}{c} = A \frac{2}{3} \rho_0 k \ , \tag{41}$$

so that only three constants, c_l, c_τ and A have to be set. In this work the number of independent variables is reduced to two by alleging that the characteristic time scale τ_s and length scale l_s of Tam & Auriault's model are related by the convection speed u_c following,

$$\tau_s = \frac{l_s}{u_c} \ . \tag{42}$$

The value of $u_c = 0.65u_j$ is well-acknowledged in the literature [22] to relate the integral length scale l_i to the integral time scale τ_i. It is assumed that Tam & Auriault's characteristic scales l_s and τ_s are related by the same convection speed u_c. This is a reasonable approximation, since from the expression of the autocorrelation, equation (13),

$$l_i(x) = \int_0^\infty R_{u'_x u'_x}(x,r)\mathrm{d}r = \int_0^\infty e^{-\frac{\log(2)r^2}{l_s(x)^2}}\,\mathrm{d}r = \frac{l_s(x)}{2}\sqrt{\frac{\pi}{\log(2)}} \approx 1.064\, l_s(x)\ , \tag{43}$$

the integral length scale l_i differ from l_s by only 6%. Then, from dimensional considerations, k $[m^2.s^{-2}]$ and ε $[m^2.s^{-3}]$ must be linked by a characteristic time scale of the mean flow, i.e.,

$$\varepsilon \propto k\left|\frac{\partial u_x}{\partial r}\right|\ . \tag{44}$$

From equations (41) and 44), l_s can then be determined without the turbulent dissipation rate ε with,

$$l_s \propto \sqrt{k}/\left|\frac{\partial u_x}{\partial r}\right|\ . \tag{45}$$

The integral length scale l_i has been computed along the lip-line from $R_{u'_x u'_x}$, the autocorrelation of the fluctuating axial velocities calculated in the LES (see acknowledgements). It is used to calibrate the proportionality constant of equation (45) with regards also of equation (43). The length scales l_s along the lip-line corresponding to the best fit are presented figure 9. They are shown for two meshes with element sizes of $0.2D_j$ and $0.5D_j$ the proportionality constant is 0.05.

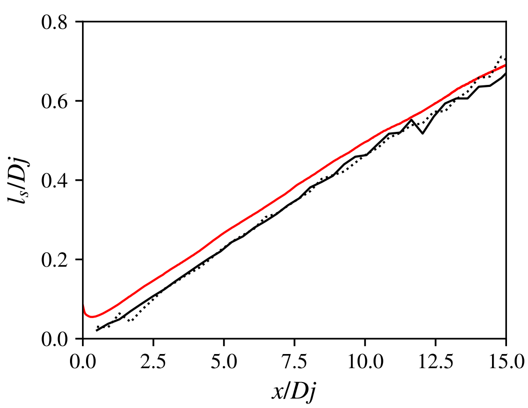

Fig. 9 Evolution of the length scale l_s along the jet lip-line. —— reference computed from the LES flow solution. Best fit for l_s computed with equation (45) considering a proportionality constant of 0.05, for computational aeroacoustic grids with element sizes of, ······ $0.5D_j$, and, —— $0.2D_j$.

To calibrate the amplitude A of the source term's autocorrelation introduced by the equations (41) and (13), the noise spectra measured at 90^o in the far field of a round jet is taken as reference. Because the diameter of the jet D_j used in the LES solution differs from the experimental one, the sound power levels (SPL) measured, and the computed one, are normalised to a distance of 1 m and compensated so as to correspond to an equivalent jet of diameter 1 m^2. The noise spectra are both expressed in dB/St. The Fourier transform of the pressure autocorrelation S_{pp} obtained with Tam & Auriault's formula, equation (26), is hence related with the normalised SPL by,

$$SPL(dB/St) = 10\log_{10}\left(\frac{S_{pp}(\boldsymbol{x}_m,\omega)}{p_{\mathrm{ref}}^2}\right) + 10\log_{10}\left(\frac{u_j}{D_j}\right) - 10\log_{10}\left(\frac{\pi D_j^2}{4}\right) + 10\log_{10}\left(|\boldsymbol{x}_m|^2\right)\ , \tag{46}$$

where $p_{\mathrm{ref}} = 20.0\,\mu$Pa and $|\boldsymbol{x}_m|$ corresponds to the distance from the jet exhaust to the microphone position. Note moreover, that the `pwelch()` function of *Matlab* used in many signal processing treatments, as for the measured spectra considered here, considers a different Fourier transform convention than the one leading to equation (14). Furthermore, if a real-valued signal p is considered, *Matlab*'s `pwelch()` is 'one-sided' and from the Fourier transform convention considered by this function, $\texttt{pwelch}(p) = \frac{2}{2\pi}\mathrm{E}\left[\hat{p}^*(f)\hat{p}(f)\right] = \frac{1}{\pi}\int_{-\infty}^{\infty} R_{pp}(\tau)e^{i\omega\tau}\mathrm{d}\tau$. So that in the end, there is additionally a $10\log_{10}(\pi)$ term difference between both conventions. The graphs of this paper are plotted with the convention of `pwelch()`.

At 90^o of the jet axis, the jet mean flow refraction effects are deemed not of primary significance and in a configuration without external wind, Green's function found in Tam & Auriault's formula expresses simply,

$$|\mathrm{D}_{-\boldsymbol{u}_0,\boldsymbol{x}_m}(\phi^\dagger_{\boldsymbol{x}_m})|^2 = \frac{\omega^2}{16\pi^2 a_0^4 |\boldsymbol{x} - \boldsymbol{x}_m|^2} . \tag{47}$$

Details to this expression are provided in the appendix paragraph. This analytical expression of Green's function serves to calibrate the amplitude A of the sound source model. Figure 10 presents acoustic measurements at 90^o from a $M_j = 0.9$ round jet [23] together with Tam & Auriault's model evaluated with equation (47), the value of l_s and τ_s defined earlier, and the best-fit obtained for the source amplitude, that is $A = 0.0006$. Tam & Auriault's remarkably

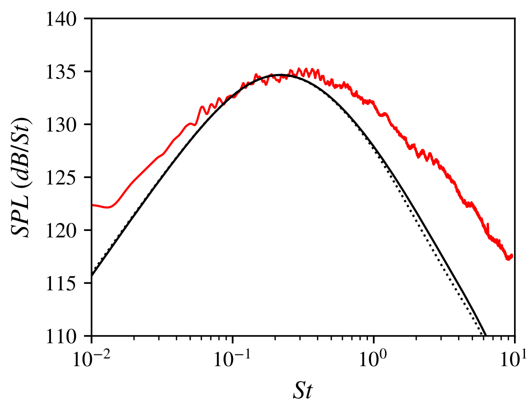

Fig. 10 Power spectral density at 90^o from the axis of a $M_j = 0.9$ round jet normalised to an equivalent distance of 1 m and to equivalent jet cross-section of 1 m^2. The analytical free-field solution is used in the mixing noise model to calibrate the sound source amplitude A, with a best-fit reached for $A = 0.0006$. —— ECL measurements [23], noise spectra obtained with Tam & Auriault's formula with a sound source interpolated on grids with elements of sizes, ······ $0.5D_j$ and, —— $0.2D_j$.

well predicts the peak center frequency and the width of the jet noise spectra when the parameters of this model l_s and τ_s are not tuned arbitrarily but informed with physical meaningful information. It is seen also how the cruelly simple analytical solution of adjoint Green's function $\phi^\dagger_{\boldsymbol{x}_m}$, equation (47), provides a reasonable prediction at 90^o from the jet axis [24, 25]. Figure 10 presents noise predictions for two different computational aeroacoustic grids with quadratic elements of size $0.5D_j$ and $0.2D_j$ showing only little differences in the predictions. The accuracy of the prediction seems not to be much influenced by the discretisation of the sound source.

C. Ninety-degree acoustic spectrum

Some results of noise spectra relying on Green's function computed with *Actran TM* are presented in this paragraph. The adjoint source is set perpendicular to the jet axis at a distance from $52D_j$ from the nozzle exit, so to comply with the position of the microphone in the experimental campaign that serves as reference for this study [23]. Adjoint Green's function are computed for a sample of 100 Strouhal numbers, equispaced in a logarithmic scale between $St = 0.01$ and $St = 10$. Both PML and IE with order of 20 are investigated to achieve the truncation of the numerical domain, and two grids with element sizes of $0.2D_j$ and $0.1D_j$ are considered. Table 1 gives indicative figures on the computational cost on both grids considering MUMPS algorithm and single precision. A Xenon-Intel E5-2699 @ 2.20 GHz with 14 threads & 3 procs was used for the computation presented here. Multi-threading is used to reduce computational time [17], note that it is possible to swap on the disk to solve larger problems.

Figure 11 and figure 12 present extracts of adjoint Green's function $\phi^\dagger_{\boldsymbol{x}_m}$ in the symmetry plane of the propagation problem for the Strouhal number of $St = 0.15$ and $St = 0.60$. The real part and the absolute part - which is of relevance

element size	NRBC	DOF	RAM	time per freq.	time for 100 freqs.
$0.2D_j$	IE (order 20)	1.7×10^6	17 GB	3 min	73 CPU.h
$0.2D_j$	PML	1.7×10^6	13 GB	2.5 min	62 CPU.h
$0.1D_j$	PML	7.7×10^6	75 GB	30 min	655 CPU.h

Table 1 Computational cost for the grids considered using MUMPS solver and sequential computation.

for equation (26) - of the adjoint solution are shown for the finest grid. While for $St = 0.15$ adjoint wave fronts are spherical and do not seem to be influenced by the presence of the flow, the adjoint field is complex for $St = 0.60$ in the vicinity of the jet flow. Considering the absolute part of the adjoint field 12 a modal structure is visible in the potential core of the jet. This particular structure of adjoint Green's function will weight some areas of the mixing layer of the jet that will as a result contribute more to the observer location for this particular frequency. This is a phenomenon that is probably hardly tractable by analytical means.

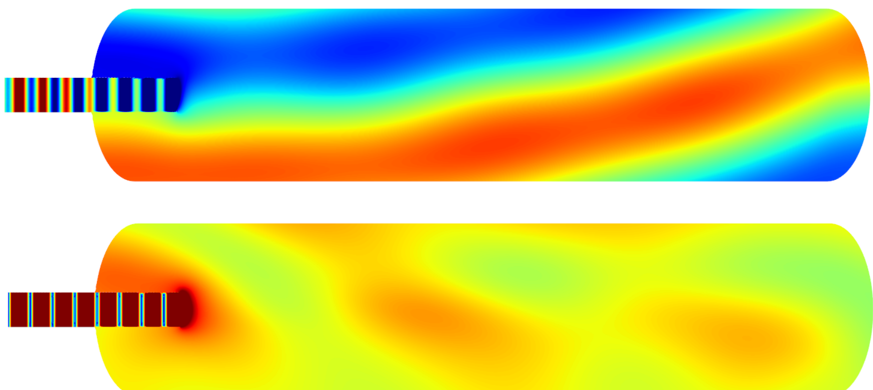

Fig. 11 Contour of adjoint Green's function $\phi^{\dagger}_{x_m}$ obtained for $St = 0.15$ on the mesh with elements of size $0.1D_j$ using PML. The real part (top) and the absolute part (bottom) are shown with identical colormaps.

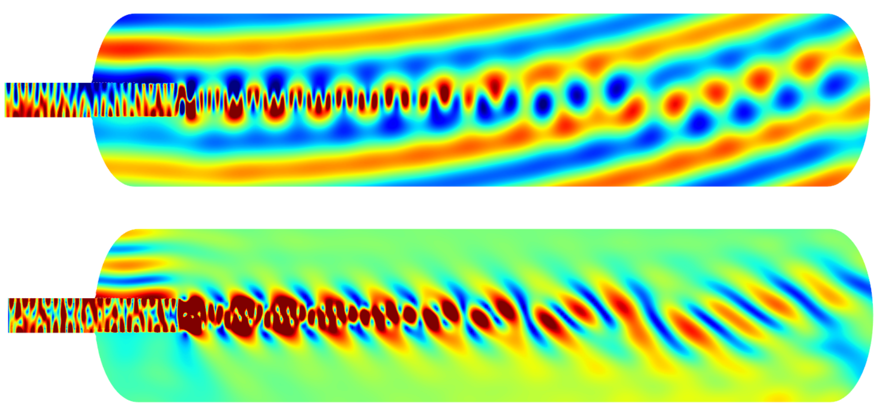

Fig. 12 Contour of adjoint Green's function $\phi^{\dagger}_{x_m}$ obtained for 38530Hz $St = 0.60$ on the mesh with elements of size $0.1D_j$ using PML. The real part (top) and the absolute part (bottom) are shown with identical colormaps.

Figure 13 presents the predictions obtained for the grids visible in figure 8 with elements of size $0.2D_j$ and $0.1D_j$ respectively. Measurements [23] and the noise spectra obtained with Tam & Auriault's formula when the free-field analytical solution, equation (47), is considered serve as references.

Computations with PML, and IE with an order of 20, have been carried out on the coarser mesh. The cut-off Strouhal numbers for this mesh with elements of size $0.2D_j$ are $St^o_{\max} \sim 1.1$ and $St^c_{\max} \sim 0.1$. Below $St^c_{\max} \sim 0.1$ a perfect agreement with the noise spectra obtained with the analytical expression of adjoint Green's function is obtained. As can be seen in figure 11, the adjoint solution does not differ qualitatively much from the free-field solution, and the noise spectra with numerical Green's functions is identical to the one based on the analytical solution. Above $St^o_{\max} \sim 1.1$, numerical error become significant and results are not reliable. Up to a Strouhal number of $St \sim 1$, which corresponds approximately to $St^o_{\max}$, the predictions on the coarse mesh with both NRBC are very alike. This tends to indicate a correct truncation of the numerical domain with both methods.

A computation with PML is executed considering the finer mesh with elements of size $0.1D_j$ and the corresponding noise spectra is plotted in figure 13. Identical predictions are obtained for $St < 0.2$, however the sequence of peaks between $St = 0.2$ and $St = 0.01$, differ from those obtained with the calculations done on the coarser mesh. This highlights the need of a mesh convergence study even though these are small discrepancies. Even for Strouhal numbers higher than $St^o_{\max}$, a very satisfactory agreement between the predictions on this finer mesh and the one based on the analytical solution is obtained. A preliminary investigation has shown that the hump shape of the noise spectra is dominated in the high frequency limit by the parameters of the sound source, while for the lower frequencies, the Green's function's dynamic dominates the noise spectra shape. This is a probable explanation for the reasonable predictions obtained for Strouhal numbers greater than $St^o_{\max}$.

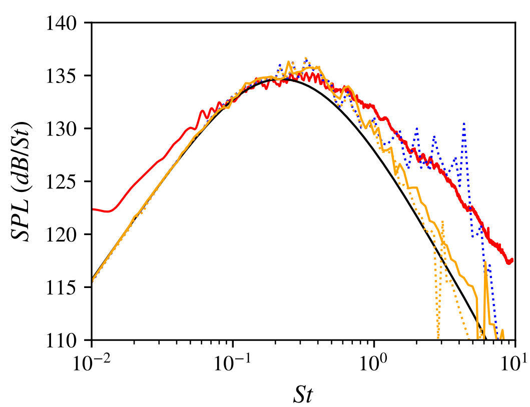

Fig. 13 Power spectral density at 90^o from the axis of a $M_j = 0.9$ round jet normalised to an equivalent distance of 1 m and to equivalent jet cross-section of 1 m^2. —— ECL measurements [23] are compared to predictions of Tam & Auriault's model, —— considering the free-field analytical expression, and considering numerical Green's functions obtained —— for the grid with elements of size $0.1D_j$ and PML, as well as for the mesh with elements of size $0.2D_j$, ······ using PML and, ······ considering IE of order 20.

VII. Conclusion

In this contribution the mixing noise model of Tam & Auriault [3] is recalled and recast for Pierce's wave equation which is twofold stable and self-adjoint. Because this potential acoustic wave equation is self-adjoint, its adjoint solution can be computed with the flow reversal theorem (FRT) [8]. A procedure to transform the equation solved by *Actran TM* into Pierce's equation is used and validated for a stratified and strongly sheared flow. In adjoint-based statistical jet noise models, Green's function are evaluated from the microphone position and the reciprocity principle is used. A procedure to set the adjoint source in the exterior of the computational domain is proposed with *Actran TM*. Some guidelines for the definition of the numerical setup are provided.

A $M_j = 0.9$ round jet is considered for the implementation of the method. Tam & Auriault's sound source parameter are calibrated based on the integral length scale computed with a LES, and very reasonable predictions have been obtained at 90^o based on physical parameters and the simple free-field analytical solution. Adjoint Green's functions are computed with *Actran TM*. Complex features in Green's functions are observed at frequencies close to the peak frequency of the jet. While consistent predictions with those obtained with the analytical solution have been obtained, a mesh convergence study is still required for more confidence in the results presented here. Nevertheless, the implementation of the methodology considering numerical adjoint Green's functions for Pierce's wave equation seems readily satisfactorily validated, and more complex configuration may now be tackled. A significant asset of the formulation, as presented here, is its ability to account for the presence of surfaces and of realistic jet flows in the acoustic propagation problem.

Appendix

Free-field analytical solution to Pierce's equation

In section IV.B, the squared absolute value of Green's solution of adjoint Pierce's equation $|\phi^{\dagger}_{\boldsymbol{x}_m}|^2$ and of its material derivative $|\mathrm{D}_{-\boldsymbol{u}_0,\boldsymbol{x}_m}(\phi^{\dagger}_{\boldsymbol{x}_m})|^2$ are involved in the computation of the acoustic power spectral density S_{pp}. Free-field Green's function for a medium with an uniform flow are derived here to the sake of validation. In a first approximation, only the movement of the surrounding medium is considered to model the acoustic propagation, and Pierce's adjoint equation reduces to the convected wave equation,

$$(-i\omega + \boldsymbol{u}_0 \cdot \nabla)^2 \phi^{\dagger}_{\boldsymbol{x}_m} - a_0^2 \Delta \phi^{\dagger}_{\boldsymbol{x}_m} = \delta_{\boldsymbol{x}_m} \ , \tag{48}$$

where $\delta_{\boldsymbol{x}_m}$ is an impulsive source set at the observer position. The boundary conditions of the adjoint problem are such as the solution is anti-causal, and the adjoint solution to the free-field propagation problem expresses as [8],

$$\phi^{\dagger(\boldsymbol{x})}_{\boldsymbol{x}_m} = \exp\left(-i\frac{\omega}{a_0}\frac{\boldsymbol{M}_0 \cdot (\boldsymbol{x} - \boldsymbol{x}_m)}{1 - M_0^2}\right) \frac{\exp\left(-i\dfrac{\omega}{a_0}\dfrac{r_{\boldsymbol{x}_m}}{1 - M_0^2}\right)}{4\pi a_0^2 r_{\boldsymbol{x}_m}} \ , \tag{49}$$

where $r_{\boldsymbol{x}_m} = \sqrt{(1 - M_0^2)|\boldsymbol{x} - \boldsymbol{x}_m|^2 + (\boldsymbol{M}_0 \cdot (\boldsymbol{x} - \boldsymbol{x}_m))^2}$, and $\boldsymbol{M}_0 = \boldsymbol{u}_0 / a_0$ is the vectorial Mach number. It is worth remembering that this solution is such as the reciprocity principle is fulfilled,

$$\phi^{\dagger(\boldsymbol{x})}_{\boldsymbol{x}_m} = \phi^{(\boldsymbol{x}_m)\,*}_{\boldsymbol{x}} \tag{50}$$

Then by choosing the axis in such a way that the flow is oriented along the first direction, the material derivative $\mathrm{D}_{-\boldsymbol{u}_0,\boldsymbol{x}_m}\left(\phi^{\dagger}_{\boldsymbol{x}_m}\right)$, expresses as,

$$\mathrm{D}_{-\boldsymbol{u}_0,\boldsymbol{x}_m}\left(\phi^{\dagger(\boldsymbol{x})}_{\boldsymbol{x}_m}\right) = -i\omega\phi^{\dagger(\boldsymbol{x})}_{\boldsymbol{x}_m} - u_{0,1}\frac{\partial \phi^{\dagger(\boldsymbol{x})}_{\boldsymbol{x}_m}}{\partial x_1} = \left(-i\omega + i\omega\frac{M_0}{1 - M_0^2}\left(M_0 + \frac{\partial r_{\boldsymbol{x}_m}}{\partial x_1}\right) + \frac{u_{0,1}}{r_{\boldsymbol{x}_m}}\frac{\partial r_{\boldsymbol{x}_m}}{\partial x_1}\right)\phi^{\dagger(\boldsymbol{x})}_{\boldsymbol{x}_m} \ , \tag{51}$$

where $\partial r_{\boldsymbol{x}_m}/\partial x_1 = (x_1 - x_{m,1})/r_{\boldsymbol{x}_m}$, $\boldsymbol{x} = (x_1, x_2, x_3)^T$, $\boldsymbol{x}_m = (x_{m,1}, x_{m,2}, x_{m,3})^T$ and $\boldsymbol{u}_0 = (u_{0,1}, u_{0,2}, u_{0,3})^T$. A $(2\pi)^2$ difference with respect to the analytical solution derived in [24, eq. (49)-(50)] is noted.

Acknowledgement

The authors benefited from insightful discussions with Christophe Bogey, who moreover provided the mean flow data computed from large-eddy simulation used in this study. This work was performed within the framework of the AMBROSIA project founded by The French Civil Aviation Authority (DGAC Convention 2019-18), with also the support of the Labex CeLyA of the Université de Lyon, within the programme "Investissements d'Avenir" (ANR-10-LABX-0060/ANR-11-IDEX-0007) operated by the French National Research Agency (ANR).

References

[1] Tam, C. K. W., and Auriault, L., "Mean flow refraction effects on sound radiated from localized source in a jet," *Journal of Fluid Mechanics*, Vol. 370, 1998, pp. 149–174.

[2] Pierce, A. D., "Wave equation for sound in fluids with unsteady inhomogeneous flow," *The Journal of the Acoustical Society of America*, Vol. 87, No. 6, 1990, pp. 2292–2299.

[3] Tam, C. K. W., and Auriault, L., "Jet mixing noise from fine-scale turbulence," *AIAA Journal*, Vol. 37, No. 2, 1999, pp. 145–153.

[4] Béchara, W., Lafon, P., Bailly, C., and Candel, S. M., "Application of a κ-ε turbulence model to the prediction of noise for simple and coaxial free jets," *The Journal of the Acoustical Society of America*, Vol. 97, No. 6, 1995, pp. 3518–3531.

[5] Morris, P. J., and Miller, S. A. E., "Prediction of broadband shock-associated noise using Reynolds-averaged Navier-Stokes computational fluid dynamics," *AIAA Journal*, Vol. 48, No. 12, 2010, pp. 2931–2944. https://doi.org/10.2514/1.J050560, URL http://arc.aiaa.org/doi/10.2514/1.J050560.

[6] Mosson, A., Binet, D., and Caprile, J., "Simulation of the installation effects of the aircraft engine rear fan noise with ACTRAN/DGM," *20th AIAA/CEAS Aeroacoustics Conference*, AIAA Paper 2014-3188, Atlanta, Georgia, 2014. https://doi.org/10.2514/6.2014-3188.

[7] Möhring, W., "A well posed acoustic analogy based on a moving acoustic medium," *Aeroacoustic workshop SWING*, Dresden, 1999.

[8] Spieser, É., and Bailly, C., "Sound propagation using an adjoint-based method," *Journal of Fluid Mechanics*, Vol. 900, 2020, p. A5. https://doi.org/10.1017/jfm.2020.469.

[9] Tam, C. K. W., Golebiowski, M., and Seiner, J., "On the two components of turbulent mixing noise from supersonic jets," *2nd AIAA/CEAS Aeroacoustics Conference*, AIAA Paper 1996-1716, State College, Pennsylvania, 1996. https://doi.org/10.2514/6.1996-1716.

[10] Ribner, H. S., "Quadrupole correlations governing the pattern of jet noise," *Journal of Fluid Mechanics*, Vol. 38, No. 1, 1969, pp. 1–24.

[11] Lighthill, M. J., "On sound generated aerodynamically I. General theory," *Proceedings of the Royal Society of London. Series A. Mathematical and Physical Sciences*, Vol. 1107, The Royal Society London, 1952, pp. 564–587.

[12] Lielens, G., Free Field Technologies, personnal communication, Mont-Saint-Guibert, 11/09/2019.

[13] Spieser, E., "Adjoint-based jet noise propagation model for the acoustic potential," Ph.D. thesis, École centrale de Lyon, Laboratoire de Mécanique des Fluides et d'Acoustique (LMFA) - CIFRE Safran Aircraft Engines, N° 2020LYSEC43, 2020. https://acoustique.ec-lyon.fr/publi/spieser_thesis.pdf.

[14] Free Field Technologies, S. A., *Actran 19.0 User's Guide Volume 1 Installation, Operations, Theory and Utilities*, MSC Software Company, 2018.

[15] Free Field Technologies, S. A., *Actran 19.0 User's Guide Volume 2 Extended DAT (EDAT) Input File Syntax*, MSC Software Company, 2018.

[16] Dahl, M. D., "Fourth CAA workshop on benchmark problems," Tech. Rep. 2004-212954, NASA, 2004.

[17] Van Antwerpen, B., Detandt, Y., Copiello, D., Rosseel, E., and Gaudry, E., "Performance improvements and new solution strategies of Actran TM for nacelle simulations," *20th AIAA/CEAS Aeroacoustics Conference*, AIAA Paper 2014-2315, Atlanta, Georgia, 2014. https://doi.org/10.2514/6.2014-2315.

[18] Astley, R. J., Macaulay, G. J., Coyette, J.-P., and Cremers, L., "Three-dimensional wave-envelope elements of variable order for acoustic radiation and scattering. Part I. Formulation in the frequency domain," *The Journal of the Acoustical Society of America*, Vol. 103, No. 1, 1998, pp. 49–63.

[19] Ruggiero, A., D'Amato, R., and Affatato, S., "Comparison of meshing strategies in THR finite element modelling," *Materials*, Vol. 12, No. 14, 2019, p. 2332.

[20] Bogey, C., "Grid sensitivity of flow field and noise of high-Reynolds-number jets computed by large-eddy simulation," *International Journal of Aeroacoustics*, Vol. 17, No. 4-5, 2018, pp. 399–424. https://doi.org/10.1177/1475472X18778287.

[21] Bogey, C., "Acoustic tones in the near-nozzle region of jets: characteristics and variations between Mach numbers 0.5 and 2," *Journal of Fluid Mechanics*, 2021. https://doi.org/10.1017/jfm.2021.426.

[22] Harper-Bourne, M., "Jet noise turbulence measurements," *9th AIAA/CEAS Aeroacoustics Conference*, AIAA Paper 2004-3214, 2003. https://doi.org/10.2514/6.2003-3214.

[23] Bogey, C., Barré, S., Fleury, V., Bailly, C., and Juvé, D., "Experimental study of the spectral properties of near-field and far-field jet noise," *International Journal of Aeroacoustics*, Vol. 6, No. 2, 2007, pp. 73–92.

[24] Morris, P. J., and Farassat, F., "Acoustic analogy and alternative theories for jet noise prediction," *AIAA Journal*, Vol. 40, No. 4, 2002, pp. 671–680.

[25] Goldstein, M. E., "Ninety-degree acoustic spectrum of a high speed air jet," *AIAA Journal*, Vol. 43, No. 1, 2005, pp. 96–102.